Geochemical Journal, Vol. 48, pp. 19 to 28, 2014 doi:10.2343/geochemj.2.0281

Isotope geochemistry and its implications in the origin of Yangla copper deposit, western Yunnan, China

XI-AN YANG,[1,2,3] JIA-JUN LIU,[4]* SI-YU HAN,[4] GUO-HAO JIANG[5] and DE-GAO ZHAI[4]

[1]Institute of Mineral Resources, Chinese Academy of Geological Sciences, 26 Baiwanzhuang Street, Beijing 100037, China
[2]Chinese Academy of Geological Sciences, 26 Baiwanzhuang Street, Beijing 100037, China
[3]MLR Key Laboratory of Metallogeny and Mineral Assessment, Institute of Mineral Resources, Chinese Academy of Geological Sciences, Beijing 100037, China
[4]State Key Laboratory of Geological Process and Mineral Resources, China University of Geosciences, Beijing 100083, China
[5]State Key Laboratory of Ore Deposit Geochemistry, Institute of Geochemistry, Chinese Academy of Sciences, Guiyang 550002, China

(*Received June 18, 2013; Accepted September 12, 2013*)

The Yangla copper deposit is located in western Yunnan Province, China, with an estimated Cu reserve of approximately 1.2 million tons. It is a typical giant copper deposit, and its mining started only recently. The $\delta^{13}C_{V-PDB}$ values of the calcites studied vary from –5.1‰ to 1.0‰, implying that the hydrothermal fluids from which the calcites precipitated were derived from the granitic magma. The $\delta^{18}O_{SMOW(H2O)}$ and δD_{SMOW} values of quartz fluid inclusions range from 0.11‰ to 2.50‰ and from –120‰ to –100‰, respectively. These data may suggest the following: (1) mixing between meteoric and magmatic fluids, or (2) the evolution of meteoric fluid by its interaction with igneous or metamorphic rocks. The $\delta^{34}S$ values of sulfides range from –4.20‰ to 1.85‰ (average: –0.85‰), which is consistent with the magmatic origin. Based on the $^{3}He/^{4}He$ ratios of fluid inclusions trapped in sulfides of the deposit (0.14–0.17 *Ra*) and $^{40}Ar/^{36}Ar$ ratios of 301–1053, it can be inferred that the ore-forming fluids of the deposit were derived primarily from the crust with a minor mantle component during the metallogenic processes. Based on C, H, O, and S isotopic compositions, and the Yangla copper deposit is bordered primarily by gently dipping thrust faults near the Linong granodiorite. Moreover, the $^{187}Re–^{187}Os$ isochron age of molybdenite puts the time of metallogenesis at 233.3 ± 3 Ma, which is virtually coeval with the emplacement of the Linong granodiorite (235.6–234.1 Ma) and highlights the genetic link between the Yangla copper deposit and the Linong granodiorite. It is likely that the ore-forming fluids exsolved from the Linong granodiorite, which was formed by crustal melting induced by the intrusion of mantle-derived magma. During the late Early Permian, the Jinshajiang oceanic plate was subducted to the west, resulting in the formation of a series of gently dipping thrust faults in the Jinshajiang tectonic belt. Subsequently, the thrust faults was tensional during the early Late Triassic, which was a time of transition from collision-related compression to extension in the Jinshajiang tectonic belt; such conditions produced an environment favorable for the formation of ore fluids. This extension, in turn, induced the upwelling of hot asthenosphere, triggering intense melting in the lithospheric mantle and producing voluminous basaltic magma. Subsequently, the mantle-derived magma likely ascended along the fractures and faults to underplate the lower crust, which underwent partial melting to generate voluminous granitic magma. After the magma reached the base of the early-stage Yangla granodiorite, the platy granodiorite at the base of the Yangla body shielded the late-stage magma. Then, this magma cooled slowly, releasing some of its ore-forming fluids into the gently dipping thrust faults near the Yangla granodiorite and producing mineralization.

Keywords: Yangla, copper deposit, isotopes, western Yunnan

INTRODUCTION

The Yangla copper deposit is located in the Yangla region of the Hengduan Mountains in Deqin County, Yunnan Province, China. The deposit has 1.2 million tons copper reserves (Yang, 2009); the region offers great potential for further exploration because of its location in the Jinshajiang tectonic zone (Pan *et al*., 2001). Previous studies have focused on the stratigraphic schemes for the Yangla region (He *et al*., 1998; Qu *et al*., 2004; Zhu *et al*., 2009a), type of deposits present (Lu *et al*., 1999; Wei *et al*., 2000), geochemistry of the Yangla granite (Wei *et al*., 1997, 2000), and geochronology of the Yangla granite (Wang *et al*., 2010). Though the systematic study of the source of the ore-forming materials of the deposit is of great significance, it has not yet been conducted. To

*Corresponding author (e-mail: liujiajun@cugb.edu.cn)

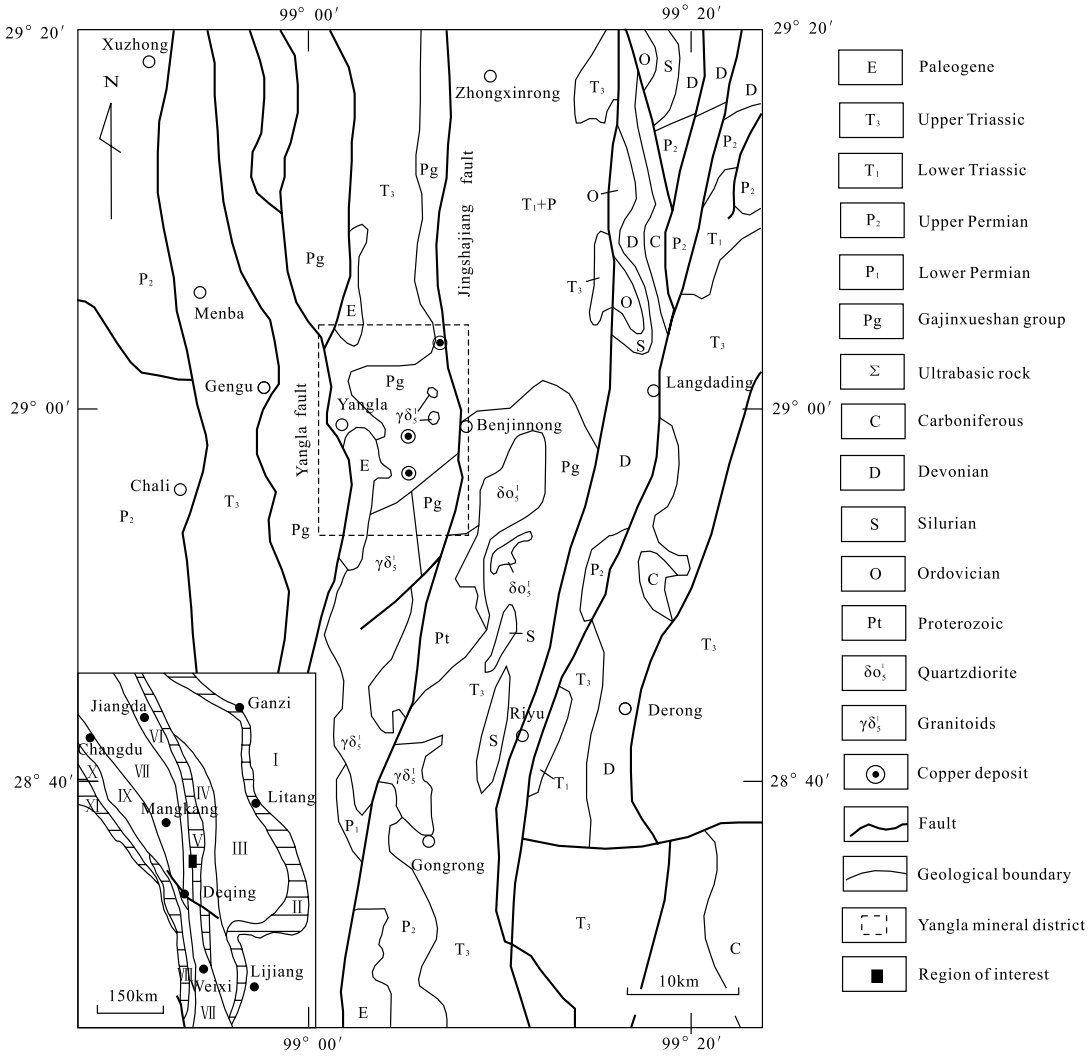

Fig. 1. Geological map of Yangla copper deposit (modified from Qu et al., 2004). I, Yangtze block; II, Ganzi–Litang melange belt; III, Yidun arc belt; IV, Zhongza–Zhongdian block; V, Jinshajiang tectonic belt; VI, Jiangda–Weixi arc belt; VII, Changdu–Simao block; VIII, Lancangjiang melange belt; IX, Chayu block; X, Tuoba–Yanjing arc belt; XI, Nujiang melange belt.

address this, the present study investigates the isotopic geochemistry (C, H, O, He, and Ar) of the Yangla copper deposit and discusses its constraints on ore genesis and the origins of ore-forming materials.

GEOLOGY OF YANGLA COPPER DEPOSIT

The Yangla copper deposit is located in the middle part of the Jinshajiang tectonic belt, between the Zhongza–Zhongdian and Changdu–Simao plates, and has experienced multiple tectonic processes (e.g., rifting, extension, subduction, and continent–continent collision) during the geological evolution of the Jinshajiang–Lancangjiang–Nujiang region. In particular, the Jinshajiang tectonic belt has been subjected to intense compression; consequently, the rocks of this region are fragmented and well-developed geological structures are abundant. However, no stratigraphy has been preserved: the various rock types occur only as fragments (Feng *et al*., 1999) that exhibit no common stratigraphy, occurring instead as mélange (Qu *et al*., 2004). Previous studies have proposed various stratigraphic schemes for the Yangla region (He *et al*., 1998; Qu *et al*., 2004; Zhu *et al*., 2009a). The surface rocks are dominated by the Gajinxueshan Group, which is a suite of sedimentary rocks that includes quartz schist, biotite-plagioclase gneiss, metasandstone, quartzite, marble, slate, siliceous rocks, volcaniclastics, and andesite, with ages ranging from Neoproterozoic to Carboniferous. The Yangla ore deposit is hosted in the Devonian Jiangbian suite (marble interlayered with sericite–quartz

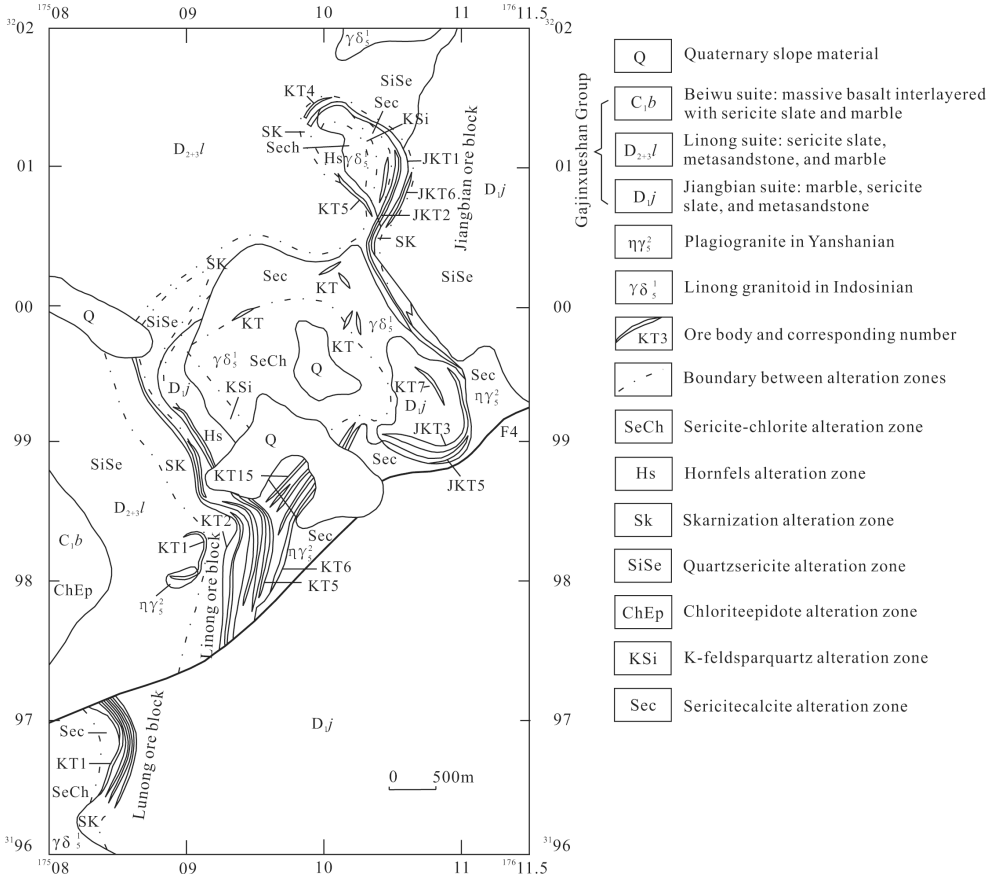

Fig. 2. Geological sketch map of Yangla copper deposit (after Yang, 2009).

schist and amphibole-bearing andesite), Devonian Linong suite (sericite slate, metasandstone, and marble), and Early Carboniferous Beiwu suite (compact massive basalt, almond-like basalt, tuff, and interlayered sericite-bearing slate and marble) (Fig. 1).

The Yangla copper deposit is located near the N–S-striking Jinshajiang and Yangla faults. These faults were active during the Caledonian orogeny, were subducted and subjected to compression during the Indosinian orogeny, and were reactivated as left-stepping strike-slip faults during the Himalayan orogeny. Second-order faults (dipping to the NW) formed during the Himalayan orogeny, several kilometers long and tens of meters wide. These second-order faults, most of which are thrust or strike-slip faults, intersect each other (Gan *et al*., 1998; Zhan *et al*., 1998).

Granitic intrusions are exposed in the Yangla region, which trends N–S in the western part of the Jinshajiang tectonic zone, typically occurring as granite stocks. The main granitic intrusions are the Indosinian Linong granodiorite and the Yanshanian plagiogranite. The Linong granodiorite is located in the middle of the Yangla ore district and is offset by the F4 fault (Fig. 2); the granodiorite body is 2 km long (N–S) and 1.5 km wide (E–W) at the surface, covering an area of 2.64 km^2. Most of the intrusion is overlain by Quaternary sediments, resulting in the irregular outcrop of the intrusive body at the surface. The wall rock is composed of the Devonian Linong suite and the Jiangbian suite, both of which occur as xenoliths in the Linong granodiorite. The granodiorite can be divided into marginal facies (40% of the total surface area) and central facies (60%), separated by a transition zone. The grain size of the granodiorite varies from medium-fine to medium-coarse and its composition varies from intermediate at the center to acid at the margin. This granitic belt intruded the Gajinxueshan Group, resulting in wall rock alteration in the form of hornfels and skarn and producing fine veins of copper mineralization and disseminated copper deposits.

The granodiorite is off-white, subhedral and medium-coarse grained; it exhibits both compact massive and banded structure. The mineral assemblage is plagioclase (40%), K-feldspar (15%), quartz (25%), amphibole (15%), and biotite (5%), with minor zircon and apatite. The

plagioclase is primarily zoned andesine, and alteration is dominated by sericitization, amphibolization, and biotitization, with local chloritization and prehnitization. The granodiorite represents the central facies of the Linong bodies.

The monzonitic granite is off-white to light yellow, subhedral and medium-fine grained, with porphyritic texture locally and a compact massive structure. The mineral assemblage is plagioclase (30%), quartz (30%), K-feldspar (25%), biotite (10%), and amphibole (5%). Alteration consists of argillization, carbonatization, and biotitization, with chloritization locally. This granite represents a marginal facies of the Linong bodies.

The Yangla copper deposit is divided into three ore blocks: the Jiangbian, Linong, and Lunong blocks. The Linong ore block is the largest, and the KT2 and KT5 orebodies of this block are the only parts of the Yangla copper deposit to be mined to date. KT2 and KT5 are bordered by a series of gently dipping imbricate thrust faults. The orebodies dip 20–40° to the west and the average grade of copper in the ore is 1.03%. The hanging wall and footwall of the orebodies consist of quartz sandstone, marble, sericite slate, and granodiorite. The most abundant ore minerals are chalcopyrite, pyrite, bornite, chalcosine, pyrrhotite, galena, sphalerite, and magnetite. The oxidized ore consists of malachite, azurite, tenorite, and limonite, and the gangue minerals include diopside, actinolite, garnet, quartz, calcite, mica, and feldspar. The ore exhibits several types of texture (subhedral grains, grains, sponge-like texture, stripes, cracks, and porphyritic texture) and structure (e.g., compact massive, disseminated, and fine veiny structures).

Samples and Analytical Methods

Different types of quartz and calcite veins are present within the reefs; however, not all of these are associated with copper mineralization. Careful field study has revealed at least three types of veining: (1) early barren quartz veins; (2) sulfide–quartz veins associated with widespread growth of pyrite, chalcopyrite, and pyrrhotite, either disseminated or concentrated in quartz veins; and (3) some late calcite veins. Of these, only the sulfide–quartz veins (which account for the majority of Cu mineralization at Yangla) and the late calcite veins were used for isotope geochemistry studies. Quartz samples YL-8-1, YL-8-2, YL-8-3, YL-24-1, YL-24-2, YL-24-3, YL-39-1, YL-39-2, YL-39-3, YL-40-1, YL-40-2, YL-40-3, YL-41-1, YL-41-2, and YL-41-3 were collected from the KT2 orebody of the Linong ore block (Table 2). Quartz samples YL-57-1, YL-57-2, and YL-57-3 were collected from the KT5 orebody of the Linong ore block (Table 2). Sulfide samples YL-34 and YL-37 were collected from the KT2 orebody of the Linong ore block, and sulfide samples YL-45, YL49, YL50, and YL53 were collected from the KT5 orebody of the Linong ore block (Table 3). The calcite samples were collected from the KT5 orebody of the Linong ore block (Table 1). The samples were crushed and the minerals were handpicked under a binocular microscope. Then, C, H, O, He, and Ar isotopic compositions were measured to constrain the source of the ore-forming fluids.

Table 1. C isotopic composition of calcites from Yangla copper deposit

Sample No.	Location	Mineral	$\delta^{13}C_{PDB}$ (‰)
YL-43-1	Calcite vein in the KT5 orebody from the Linong ore block	calcite	–3.5
YL-43-2		calcite	–4.0
YL-43-3		calcite	–3.6
YL-43-4		calcite	–3.8
YL-56-1		calcite	–5.1
YL-56-2		calcite	0.5
YL-56-3		calcite	–3.7
YL-56-4		calcite	0.4
YL-58-1		calcite	1.0
YL-58-2		calcite	0.4
YL-58-3		calcite	0.2
YL-58-4		calcite	0.7
YL-58-5		calcite	0.3

The carbon compositions of 13 calcite samples were analyzed on the MAT 251 mass spectrometer at the State Key Laboratory of Geological Process and Mineral Resources, China University of Geosciences, Beijing, China. Carbon isotopic analyses were conducted using CO_2 liberated from powdered carbonates using 100% phosphoric acid or that released from fluid inclusions in quartz separates by thermal decrepitation. CO_2 was collected, condensed, and separated in a liquid nitrogen-alcohol cooling trap (–70°C) for $\delta^{13}C$ mass spectrometry analysis. Total uncertainties were estimated to be better than ±0.2‰ for $\delta^{13}C$ (Chen *et al*., 2008).

The hydrogen and oxygen isotopic compositions of 18 samples were analyzed on the MAT 252 mass spectrometer at the Stable Isotope Laboratory of the Institute of Geology, Chinese Academy of Geological Sciences, Beijing, China. Further details of the analytical procedure can be found in Zhu *et al*. (2009b). The analytical error for $\delta D_{V\text{-}SMOW}$ was ±1‰ and the analytical precision for $\delta^{18}O$ was ±0.2‰.

He and Ar isotopic compositions were analyzed on an all-metal extraction line and mass spectrometer (GV5400) at the Institute of Geochemistry, Chinese Academy of Sciences, Guiyang, China. The analytical methods used here were similar to those described in Stuart *et al*. (1994, 1995). Approximately 500–1,000 mg of separated coarse (generally 0.5–1.5 mm) pyrrhotite and chalcopyrite grains were ultrasonically cleaned in alcohol, dried, then loaded

Table 2. H and O isotopic compositions of quartz from Yangla copper deposit

Sample No.	Mineral	Location	$\delta^{18}O$ (‰)	Th (°C)	$\delta^{18}O_{SMOW(H2O)}$ (‰)	δD_{SMOW} (‰)
YL-8-1	quartz	KT2 orebody	11.6	232.5	1.8	–104
YL-8-2	quartz	from the Linong ore block	11.7	232.5	1.9	–112
YL-8-3	quartz		11.4	232.5	1.6	–108
YL-24-1	quartz		11.5	248.6	2.5	–100
YL-24-2	quartz		11.1	248.6	2.1	–109
YL-24-3	quartz		11.3	248.6	2.3	–115
YL-39-1	quartz		10.6	240.4	1.2	–105
YL-39-2	quartz		10.9	240.4	1.5	–117
YL-39-3	quartz		10.8	240.4	1.4	–106
YL-40-1	quartz		11.9	221.4	1.5	–115
YL-40-2	quartz		11.5	221.4	1.1	–112
YL-40-3	quartz		11.4	221.4	1.0	–118
YL-41-1	quartz		11.7	211.0	0.7	–109
YL-41-2	quartz		11.8	211.0	0.8	–104
YL-41-3	quartz		11.1	211.0	0.1	–116
YL-57-1	quartz	KT5 orebody	11.2	240.4	1.8	–120
YL-57-2	quartz	from the Linong ore block	11.3	240.4	1.9	–113
YL-57-3	quartz		11.2	240.4	1.8	–116

$\delta^{18}O_{SMOW(H2O)}$ (‰) calculated from the equation of Matsuhisa et al. (1979).

in on-line in vacuum crushers. The samples were baked on-line at *ca*. 150°C in an ultra-high vacuum system for >24 h prior to analysis to remove any adhered atmospheric gases. Gases were released from the grains into the all-metal extraction system by sequential crushing in modified Nupro valves. The released gases were exposed to a titanium sponge furnace at 800°C for 20 min to remove the majority of the active gases (e.g., H_2O and CO_2) and then exposed to two SAES Zr–Al getters (one at room temperature and the other at 450°C) for 10 min for further purification. He was separated from Ar using an activated charcoal cold finger at liquid N_2 temperature (–196°C) for 40–60 min to trap Ar. He and Ar isotopes and their abundances were analyzed on the GV5400. Gas abundances were measured by peak height comparison with known amounts of standard air from an air bottle. He and Ar abundances and isotopic ratios were calibrated against the air bottles of 0.1 cm^3 STP air (5.2×10^{-7} cm^3 STP ^4He and 9.3×10^{-4} cm^3 STP ^{40}Ar). Procedural blanks were $<2 \times 10^{-10}$ cm^3 STP ^4He and $(2–4) \times 10^{-10}$ cm^3 STP ^{40}Ar and constituted <1% of analyses. The blanks were too low to affect calibration of the abundance measurement.

Analytical Results

C isotopic compositions

As demonstrated in Table 1, the calcite samples from calcite veins in the Linong ore block of the Yangla copper deposit exhibit considerable variation in carbon isotopic compositions, with $\delta^{13}C_{PDB}$ values ranging from –5.1‰ to 1.0‰.

H and O isotopic compositions

Hydrogen and oxygen isotopes are important indicators of the characteristics and evolution of ore fluids. The oxygen isotope ratios of waters in equilibrium with the minerals were calculated using the fractionation formulas of Matsuhisa *et al*. (1979). As shown in Table 2, the $\delta^{18}O_{SMOW(H2O)}$ and δD_{SMOW} values of quartz fluid inclusions range from 0.1‰ to 2.5‰ and from –120‰ to –100‰, respectively.

He and Ar isotopic compositions

The results of He and Ar isotope analyses of fluid inclusions in pyrrhotite and chalcopyrite from the deposit are listed in Table 3. The concentrations of ^4He and ^{40}Ar were found to be $(0.65–5.46) \times 10^{-6}$ cm^3 STP g^{-1} and $(1.65–27.9) \times 10^{-8}$ cm^3 STP g^{-1}, respectively. The large variations in noble gas concentrations probably reflect variations in fluid inclusion abundance in the studied minerals. The noble gas isotopic ratios are more consistent: $^3He/^4He$ ratios are 0.14–0.17 *Ra* (where *Ra* represents the $^3He/^4He$ ratio of air, 1.39×10^{-6}) and $^{40}Ar/^{36}Ar$ ratios are 301–1053.

Discussion

C isotopic composition of calcite and its geological implications

The C isotope geochemistry of calcite has been used previously to trace the origins of hydrothermal fluids (Ohmoto and Rye, 1970; Rye *et al*., 1974; Zheng, 1990; Zheng and Hoefs, 1993). The results of the present study show that all of the $\delta^{13}C_{PDB}$ values obtained from cal-

Table 3. He and Ar isotopic compositions of fluid inclusions in sulfides from Yangla copper deposit

Sample No.	Location	Mineral	^{40}Ar (10^{-8} cm^3 STP)	^{36}Ar (10^{-11} cm^3 STP)	$^{40}Ar/^{36}Ar$	^{4}He (10^{-6} cm^3 STP)	^{3}He (10^{-13} cm^3 STP)	$^{3}He/^{4}He$ (Ra)
YL-34	KT2 orebody	pyrrhotite	3.3 ± 0.0059	4.6 ± 0.05	712.6 ± 37.5	0.72 ± 0.015	1.75 ± 0.024	0.17 ± 0.005
YL-37	from the Linong ore block	pyrrhotite	1.7 ± 0.0058	1.6 ± 0.10	1053.0 ± 107.9	0.65 ± 0.015	1.44 ± 0.034	0.16 ± 0.006
YL-45	KT5 orebody	pyrrhotite	4.4 ± 0.0058	5.3 ± 0.09	826.4 ± 72.5	5.46 ± 0.015	12.0 ± 0.025	0.16 ± 0.005
YL-49	from the Linong ore block	pyrrhotite	1.7 ± 0.006	2.7 ± 0.09	605.7 ± 56.5	3.12 ± 0.015	6.05 ± 0.029	0.14 ± 0.005
YL-50		chalcopyrite	21.1 ± 0.0058	46.9 ± 0.13	449.3 ± 6.6	3.41 ± 0.015	7.13 ± 0.031	0.15 ± 0.005
YL-53		chalcopyrite	27.9 ± 0.0059	92.6 ± 0.01	301.2 ± 3.7	1.11 ± 0.015	2.24 ± 0.024	0.14 ± 0.004

Ra represents the $^{3}He/^{4}He$ ratio of air (1 Ra = 1.39 × 10^{-6}).

cites from the Yangla copper deposit fall within the magmatic carbon range (–10.3‰ to 2.9‰) (Craig, 1953; Ohmoto, 1972; Fuex and Baker, 1973; Rollinson, 1993; Itoh and Hanari, 2010). In contrast, the $\delta^{13}C_{PDB}$ values obtained from calcites from the marble in the Yangla copper deposit range from 3.60‰ to 4.21‰ (Pan *et al*., 2000); these values are greater than those of the Yangla copper deposit, implying that the isotopic carbon content of calcites from the primary ores was not derived from the marble.

H and O isotopic composition of quartz and its geological implications

The $\delta^{18}O_{SMOW(H2O)}$ values of fluid inclusions in quartz from the Yangla copper deposit are similar to those for the magmatic water; however, the δD_{SMOW} values of the inclusions are much lower than those for the magmatic water. Therefore, all of the data points in the δD_{SMOW}–$\delta^{18}O_{SMOW(H2O)}$ diagram fall outside the magmatic water region (Fig. 3). These data suggest the following: (1) mixing between a magmatic fluid and a meteoric fluid with δD_{SMOW} of *ca*. –200‰ and $\delta^{18}O_{SMOW(H2O)}$ of *ca*. –25‰, corresponding to precipitation at very high latitudes; or (2) evolution of a meteoric fluid with initial δD_{SMOW} of *ca*. –120‰ and initial $\delta^{18}O_{SMOW(H2O)}$ of *ca*. –16‰ owing to interaction with igneous or metamorphic rocks (Gao *et al*., 2009).

S isotopic compositions of sulfides and their geological implications

The studied sulfides have $\delta^{34}S$ values ranging from –0.90‰ to 1.85‰, with averages of 0.60‰ for pyrite, –1.35‰ for chalcopyrite (–4.20‰ to 0.96‰), and –2.02‰ for pyrrhotite (–2.60‰ to –1.2‰) (Pan *et al*., 2000; Yang *et al*., 2012); these are the most abundant ore minerals in the Yangla copper deposit. If the $\delta^{34}S$ values of these iron sulfides can be assumed to represent the total sulfur isotopic compositions of the ore-forming fluids, their S compositions may be used to trace the source magma (Vallet *et al*., 2006). The $\delta^{34}S$ values of sulfides from the deposit range from –4.20‰ to 1.85‰ (average: –0.85‰), although most are close to zero. This observation, when considered in tandem with the spatial association between the Yangla copper deposit and the Yangla granodiorite, suggests that the ore-forming fluids were mainly derived locally, i.e., from the granodiorite intrusions.

He and Ar isotopic compositions of sulfides and their geological implications

Sources of helium and argon

Cosmogenic ^{3}He Post-crystallization production of ^{3}He within a mineral can occur owing to the interaction of cosmic rays with certain nuclei, although this process is limited to the top 1.5 m of any exposed surface. However, the samples analyzed here were all collected from underground mine workings; accordingly, cosmogenic ^{3}He production in mineral lattices and fluid inclusions can be ignored (Hu *et al*., 2009).

Effects of lattice-trapped noble gases and air Ar A major advantage in using sequential crushing of minerals (as opposed to fusion) for extracting noble gases is that it promotes the preferential release of inclusion-trapped noble gases rather than those contained within the mineral lattice. Contribution of in situ-produced ^{40}Ar from the mineral lattice to the measured $^{40}Ar/^{36}Ar$ ratio is believed to be impossible owing to the low diffusivity of Ar in pyrite and the low K content of pyrites. In general, measured $^{40}Ar/^{36}Ar$ ratios are accepted to be lower than the true $^{40}Ar/^{36}Ar$ ratios of fluids owing to the contribution of atmospheric Ar. Though rigorous analytical procedures can minimize the amount of atmospheric Ar absorbed on the sample surfaces and crushing apparatus, they cannot completely eliminate the air-derived contaminants. In addition, $^{40}Ar/^{36}Ar$ is also affected by late-stage secondary fluid inclusions of atmospheric origin, which are unrelated to ore genesis. As these secondary fluid inclusions are typically distributed linearly along microfissures in the minerals, the contribution from secondary low-$^{40}Ar/^{36}Ar$ fluid inclusions reduces as crushing progresses. In the present study, the $^{40}Ar/^{36}Ar$ values of subsequent crushing steps (e.g., first vs. second crush) generally agree within error (Table 3), suggesting that

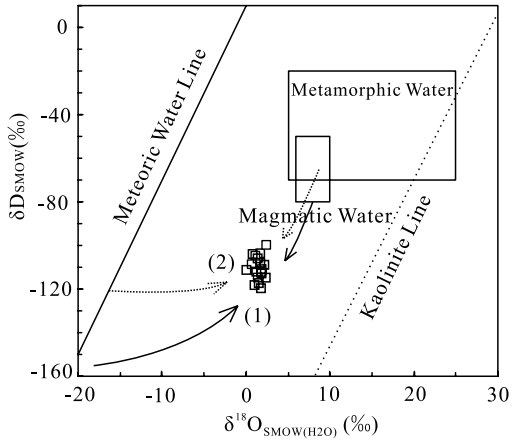

Fig. 3. δD_{SMOW}–$\delta^{18}O_{SMOW(H2O)}$ diagram of Yangla copper deposit. This distribution results from either (1) mixing between a magmatic fluid and a meteoric fluid with δD_{SMOW} of ca. –200‰ and $\delta^{18}O_{SMOW(H2O)}$ of ca. –25‰ (corresponding to precipitation at very high latitudes), or (2) evolution of a meteoric fluid with initial δD_{SMOW} of ca. –120‰ and initial $\delta^{18}O_{SMOW(H2O)}$ of ca. –16‰ by interaction with igneous or metamorphic rocks.

these samples contain few secondary fluid inclusions of atmospheric origin; this is consistent with observations of fluid inclusion morphologies in pyrite-associated quartz. Furthermore, the $^3He/^{36}Ar$ ratios ($0.2–22.5 \times 10^{-3}$) of these samples (Table 3) are much higher than those of the atmosphere or of air-saturated water ($\sim 5 \times 10^{-8}$), indicating that He in the fluids that generated the Yangla copper ores is predominantly non-atmospheric in origin. This is typical of ore fluids, because He concentrations in the atmosphere are generally too low to influence He abundances and isotopic compositions of crustal fluids (Hu *et al*., 2009).

The amount of radiogenic ^4He released from a mineral lattice depends on the grain size of the crushed minerals: the finer the minerals are crushed, the greater the surface area of the crushed grains and the more radiogenic ^4He that will be released from the mineral lattice. $^3He/^4He$ remains constant during the crushing process, suggesting that negligible radiogenic ^4He was released from the mineral lattice and/or that He diffusion through the pyrite is sufficiently slow to prevent He loss during crushing (Hu *et al*., 2009).

The pyrrhotite and chalcopyrite samples analyzed were well-formed euhedral crystals with no evidence of subsequent deformation and exhibit a paragenesis with pyrite, bornite, chalcosine, galena, and sphalerite. Therefore, the extracted fluids should represent mineralizing fluids and the measured He isotopic compositions of the samples listed in Table 3 likely represent the "initial" values of fluid inclusions or ore-forming fluids of the deposit.

Fluid characteristics

Numerous studies have shown that He and Ar gases can be used as indicators of the changing characteristics of differentiation along with degassing during Earth's evolution (Barnard *et al*., 1994a, b; Baptiste and Fougute, 1996). Thus, the He and Ar isotopes of the mantle, crust, and surface atmosphere are distinct. Of these, the mantle retains higher original He and Ar (such as ^3He and ^{36}Ar), but lower radiogenic ^4He and ^{40}Ar. Therefore, it is generally assumed that the value of $^3He/^4He$ in the continental mantle is 6–9 *Ra* (*Ra* = $^3He/^4He = 1.39 \times 10^{-6}$), that of $^{40}Ar/^{36}Ar$ is greater than 20,000, and that of $^{40}Ar/^4He$ is approximately 0.33–0.56 (Simmons *et al*., 1987; Hu *et al*., 1999). However, the value of $^3He/^4He$ in the typical crust is usually less than 0.1 *Ra*; in fact, in most cases, it is only 0.01–0.05 *Ra*. As there is abundant radiogenic ^{40}Ar in the crust, the concentration of $^{40}Ar/^{36}Ar$ often exceeds 45,000, and that of $^{40}Ar/^4He$ is generally within the range 0.16–0.25 (Simmons *et al*., 1987; Stuart *et al*., 1995; Hu *et al*., 1999; Feng *et al*., 2006). Thus, the He–Ar isotopic composition varies considerably between the crust and the mantle. Furthermore, it is usually assumed that the He–Ar isotopic composition of atmospheric saturated water is the same as that of the surface atmosphere, with $^3He/^4He$ = 1 *Ra*, $^{40}Ar/^{36}Ar$ = 295.5, and $^{40}Ar/^4He$ approximately 0.001 (Simmons *et al*., 1987; Stuart *et al*., 1995; Hu *et al*., 1999). Thus, the significant differences between the crust and the mantle reservoirs allow $^3He/^4He$, $^{40}Ar/^{36}Ar$, and $^{40}Ar/^4He$ to be used as potential tracers in identifying the source characteristics of ore-forming fluids (Shen *et al*., 2013).

The sulfides from the Yangla copper deposit exhibit $^3He/^4He$ ratios of 0.14–0.17 *Ra*, with a mean value of 0.15 *Ra* (Table 3); these values are slightly higher than those for the crust (0.01–0.1 *Ra*), but markedly lower than those for the mantle (6–9 *Ra*). All of the data points from sulfides plot between the crust and the mantle on the ^3He versus ^4He diagram (Fig. 4), although most plot closer to the crustal domain. The percentage of mantle-derived He can be calculated according to the crust-mantle mixing model, which is expressed as follows: $He = [(^3He/^4He)_{(sample)} - (^3He/^4He)_{(Crust)}]/[(^3He/^4He)_{(Mantle)} - (^3He/^4He)_{(Crust)}] \times 100$ (Xu *et al*., 1995).

The lower limits of $^3He/^4He$ for the crust and the mantle end members have been shown to be 0.01 *Ra* and 6 *Ra*, respectively (Stuart *et al*., 1995). The results presented here show that the content of mantle-derived He in the sulfides from the Yangla deposit is in the range 2.17–2.67%. In general, the $^3He/^4He$ ratios of ore fluids in the deposit are close to the crustal values, reflecting the fact that the ore fluids originated primarily from the crust and were mixed with a small amount of the mantle component during the metallogenic process.

Furthermore, the $^{40}Ar/^{36}Ar$ ratios mostly range from

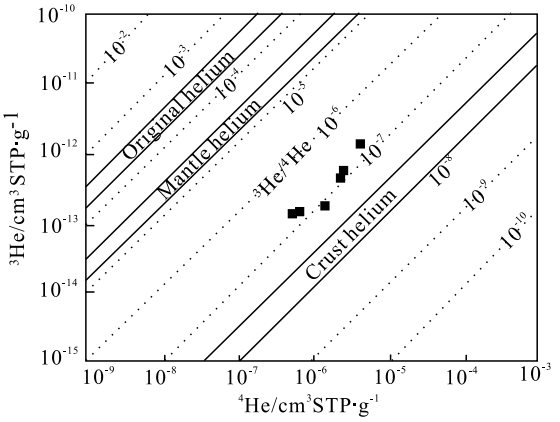

Fig. 4. He isotope composition of Yangla copper deposit.

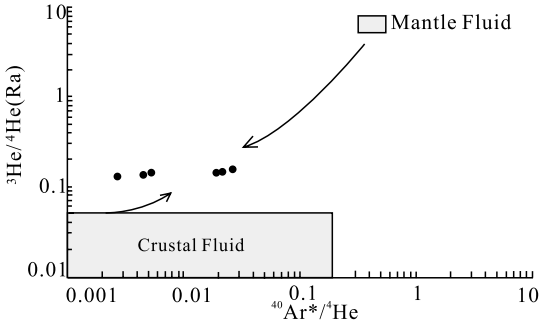

Fig. 5. $^3He/^4He$ (Ra) vs. $^{40}Ar^*/^4He$ plot of inclusion-trapped fluids from Yangla copper deposit (after Hu et al., 2009).

301.24 to 1052.99 (Table 3). These values are higher than that for the atmosphere ($^{40}Ar/^{36}Ar$ = 295.5), indicating the presence of excess argon that was likely produced by higher radiogenic ^{40}Ar. Finally, the plots of $^3He/^4He$ (*Ra*) vs. $^{40}Ar^*/^4He$ ($^{40}Ar^* = {}^{40}Ar - {}^{36}Ar \times 295.5$; Hu *et al.*, 2009) of fluids in sulfides from the deposit (Fig. 5) fall close to the field of the crustal fluid component, indicating that the ore-forming fluids include a major crustal component.

In summary, it can be inferred that the ore-forming fluids of the deposit are derived primarily from the crust, with minor input of a mantle component during metallogenesis. Based on the C, H, O, and S isotopic compositions, and the Yangla copper deposit is bordered primarily by gently dipping thrust faults near the Linong granodiorite (Fig. 2). Moreover, metallogenesis can be dated to 233.3 ± 3 Ma (Yang *et al.*, 2012) based on the $^{187}Re–^{187}Os$ isochron age of molybdenite; this is virtually coeval with the emplacement of the Linong granodiorite (235.6–234.1 Ma) (Yang *et al.*, 2013), highlighting the genetic link between the Yangla copper deposit and the Linong granodiorite. It is likely that the ore-forming fluids exsolved from the Linong granodiorite, which formed by crustal melting induced by the intrusion of mantle-derived magma. This is supported by the interpretation of Gao *et al.* (2010), which suggests that the Linong granodiorite was derived by melting of subcontinental lithospheric mantle.

Ore genesis

In the late Early Permian, the Jinshajiang oceanic plate was subducted to the west, beneath the Changdu–Simao Plate, resulting in the formation of a series of imbricate ductile shear zones; these shear zones dipped gently to the NW and were formed under conditions of E–W compression in the Jinshajiang tectonic belt (Yang *et al.*, 2012).

This was followed by slab break-off and lithospheric delamination in the early Late Triassic, removing part of the lithospheric mantle keel and resulting in a transformation in the geodynamic setting from collision-related compression to extension; accordingly, the ductile shear zones were transformed to brittle shear zones. The brittle shear zones consisted of a series of thrust faults in the Jinshajiang tectonic belt, which produced an environment favorable for the generation of ore-forming fluids. The extension, in turn, induced the upwelling of hot asthenosphere, and it was the high heat flow from this asthenospheric mantle and the associated infiltration of slab-derived fluids that triggered intense melting in the lithospheric mantle, producing voluminous basaltic magma. Subsequently, the mantle-derived magma ascended along the fractures and faults to underplate the lower crust, which underwent partial melting (induced by the underplating of basaltic magma) to generate voluminous granitic magma. The ascent and coalescence of these early Late Triassic granitic magma resulted in batholith formation throughout the Yangla and adjacent regions. The geochemical character of the Yangla granodiorite, combined with its zircon U–Pb dates of 235.6–234.1 Ma (Yang *et al.*, 2013), support the hypothesis that it was derived from crustal melting induced by the intrusion of mantle-derived magma (Gao *et al.*, 2010). After arrival of the magma at the base of the early-stage Linong granodiorite, the platy nature of the granodiorite body shielded late-stage magma. Then, the magma likely cooled slowly, with some of its ore-forming fluid entering the low-angle thrust faults near the Linong granodiorite, resulting in precipitation of the copper ore minerals.

Conclusions

(1) The $\delta^{13}C_{V-PDB}$ values of the calcites studied vary from –5.1‰ to 1.0‰, implying that the hydrothermal fluids from which the calcites precipitated were derived from the granitic magma. The $\delta^{18}O_{SMOW(H2O)}$ and δD_{SMOW} val-

ues of quartz fluid inclusions range from 0.11‰ to 2.50‰ and from –120‰ to –100‰, respectively. These data may suggest the following: (1) mixing between a magmatic fluid and a meteoric fluid with δD_{SMOW} of *ca*. –200‰ and $\delta^{18}O_{SMOW(H2O)}$ of *ca*. –25‰, corresponding to precipitation at very high latitudes; or (2) meteoric fluid with initial δD_{SMOW} of *ca*. –120‰ and initial $\delta^{18}O_{SMOW(H2O)}$ of *ca*. –16‰, which evolved by its interaction with igneous or metamorphic rocks. The $\delta^{34}S$ values of sulfides, which range from –4.20‰ to 1.85‰ (average: –0.85‰), are consistent with its derivation from a magmatic source. The $^{3}He/^{4}He$ and $^{40}Ar/^{36}Ar$ ratios of fluid inclusions trapped in sulfides from the deposit range from 0.14 to 0.17 *Ra* and from 301 to 1053, respectively, suggesting that the ore-forming fluids of the deposit were derived primarily from the crust with only minor contributions from the mantle component during metallogenesis. Considering the C, H, O, and S isotopic compositions, and the Yangla copper deposit is bordered primarily by gently dipping thrust faults near the Linong granodiorite (Fig. 2). Moreover, the metallogenesis of the Yangla Cu deposit was virtually coeval with the crystallization age of the Linong granodiorite, highlighting the genetic link between the Yangla copper deposit and the Linong granodiorite. In fact, it is likely that the ore-forming fluids exsolved from the Linong granodiorite, which was formed by crustal melting induced by the intrusion of mantle-derived magma.

(2) Slab break-off and lithospheric delamination in the early Late Triassic, resulted in a transformation in the geodynamic setting from collision-related compression to extension. This extension induced the upwelling of hot asthenosphere, which triggered intense melting in the lithospheric mantle and produced voluminous basaltic magma. Subsequently, the mantle-derived magma ascended to underplate the lower crust, which underwent partial melting to generate voluminous granitic magma. Ascent and coalescence of the early Late Triassic granitic magma resulted in batholith formation throughout the Yangla and adjacent regions. After the magma arrived at the base of the early-stage Yangla granodiorite, the platy granodiorite at the base of the body shielded the late-stage magma. Then, the magma likely cooled slowly, with some of its ore-forming fluid entering the low-angle thrust faults near the Linong granodiorite, resulting in precipitation of the copper ore minerals.

Acknowledgments—This research was jointly supported by the Postdoctoral Science Foundation of China (2013M541000), the National Basic Research Program of China (2009CB421003, 2009CB421005) and the 111 Project (Grant No. B07011). The authors thank Hirochika Sumino and an anonymous reviewer for their useful comments and constructive reviews, which significantly improved the manuscript. We express our special thanks to Masahiko Honda for highlighting ways to substantially improve an earlier version of this paper.

References

Baptiste, P. J. and Fougute, Y. (1996) Abundance and isotopic composition of helium in hydrothermal sulfides from the East Pacific Rise at 13°N. *Geochim. Cosmochim. Acta* **60**, 87–93.

Barnard, P. G., Stuart, F. M., Turner, G. and Oskarsson, N. (1994a) Air contamination of basaltic magmas: implications for high $^{3}He/^{4}He$ mantle Ar isotopic composition. *J. Geophys. Res.* **99**(B9), 17709–17715.

Barnard, P. G., Stuart, F. and Turner, G. (1994b) C–He–Ar variations within a dunite nodule as a function of fluid inclusion morphology. *Earth Planet. Sci. Lett.* **128**, 243–258.

Chen, Y. J., Pirajno, F. and Qi, J. P. (2008) The Shanggong gold deposit, eastern Qinling Orogen, China: Isotope geochemistry and implications for ore genesis. *J. Asian Earth Sci.* **33**, 252–266.

Craig, H. (1953) The geochemistry of the stable carbon isotopes. *Geochim. Cosmochim. Acta* **3**, 53–92.

Feng, C. Y., She, H. Q., Zhang, D. Q., Li, D. X., Li, J. W. and Cui, Y. H. (2006) Helium, argon, sulfur and lead isotope tracing for sources of ore-forming material in the Tuolugou cobalt (Gold) deposit, Golmud city, Qinghai province, China. *Acta Geologica Sinica* **80**, 1465–1473.

Feng, Q. L., Ge, M. C., Xie, D. F., Ma, Z. and Jiang, Y. S. (1999) Stratigraphic sequence and tectonic evolution in passive continental margin, Jinshajiang belt, northwestern Yunnan province, China. *Earth Science-Journal of China University of Geosciences* **24**, 553–557 (in Chinese with English abstract).

Fuex, A. N. and Baker, D. R. (1973) Stable carbon isotopes in selected granitic, mafic, and ultramafic igneous rocks. *Geochim. Cosmochim. Acta* **37**, 2509–2521.

Gan, J. M., Zhan, M. G., Yu, F. M., He, L. Q., Chen, S. F. and Dong, F. L. (1998) Structural deformation and its ore-control significance in Yangla copper district, Deqin, western Yunnan. *Geol. Miner. Resour. South China* **4**, 59–65 (in Chinese with English abstract).

Gao, R., Xiao, L., He, Q., Yuan, J., Ni, P. Z. and Du, J. X. (2010) Geochronology, geochemistry and petrogenesis of granites in Weixi-Deqin, West Yunnan. *Earth Science-Journal of China University of Geosciences* **35**, 186–200 (in Chinese with English abstract).

Gao, Y. Q., Liu, L. and Hu, W. X. (2009) Petrology and isotopic geochemistry of dawsonite-bearing sandstones in Hailaer basin, northeastern China. *Appl. Geochem.* **24**, 1724–1738.

He, L. Q., Zhan, M. G. and Lu, Y. F. (1998) Division of sequence stratigraphy and study on ore-bearing beds in Yangla copper orefield, western Yunnan. *Geol. Miner. Resour. South China* **3**, 37–41 (in Chinese with English abstract).

Hu, R. Z., Bi, X. W., Turner, G. and Burnar, P. (1999) He–Ar isotopes geochemistry of oreforming fluid on gold ore belt in Ailao Mountains. *Science in China (Series D)* **29**, 321–330.

Hu, R. Z., Burnard, P. G., Bi, X. W., Zhou, M. F., Peng, J. T., Su, W. C. and Zhao, J. H. (2009) Mantle-derived gaseous components in ore-forming fluids of the Xiangshan uranium deposit, Jiangxi province, China: Evidence from He, Ar and C isotopes. *Chem. Geol.* **266**, 86–95.

Itoh, N. and Hanari, N. (2010) Possible precursor of perylene in sediments of Lake Biwa elucidated by stable carbon isotope composition. *Geochem. J.* **44**, 161–166.

Lu, Y. F., Chen, K. X. and Zhan, M. G. (1999) Geochemical evidence of exhalative-sedimentary ore-bearing skarns in Yangla copper mineralization concentrated area, Deqin county, northwestern Yunnan province. *Earth Science-Journal China University of Geoscience* **21**, 191–197 (in Chinese with English abstract).

Matsuhisa, Y., Goldsmith, R. and Clayton, R. N. (1979) Oxygen isotope fractionation in the system quartz-albite-anorthite-water. *Geochim. Cosmochim. Acta* **43**, 1131–1140.

Ohmoto, H. (1972) Systematics of sulfur and carbon isotopes in hydrothermal ore deposits. *Econ. Geol.* **67**, 551–578.

Ohmoto, H. and Rye, R. O. (1970) The Bluebell Mine, British Columbia; I, Mineralogy, paragenesis, fluid inclusions, and the isotopes of hydrogen, oxygen, and carbon. *Econ. Geol.* **65**, 417–435.

Pan, J. Y., Zhang, Q., Ma, D. S. and Li, C. Y. (2000) Stable isotope geochemical characteristics of the Yangla copper deposit in western Yunnan province. *Acta Mineralogica Sinica* **20**, 385–389 (in Chinese with English abstract).

Pan, J. Y., Zhang, Q. and Ma, D. S. (2001) Cherts from the Yangla copper deposit, western Yunnan province: Geochemical characteristics and relationship with massive sulfide mineralization. *Science in China (Series D)* **44**, 237–244.

Qu, X. M., Yang, Y. Q. and Li, Y. G. (2004) A discussion on origin of Yangla copper deposit in light of diversity of ore-hosting rock types. *Mineral Deposits* **23**, 431–442 (in Chinese with English abstract).

Rollinson, H. R. (1993) *Using Geochemical Data: Evaluation, Presentation, Interpretation*. Longman Science & Technical and John Wiley & Sons, Inc., New York, 343 pp.

Rye, R. O., Hall, W. E. and Ohmoto, H. (1974) Carbon, hydrogen, oxygen, and sulfur isotope study of the Darwin lead-silver-zinc deposit, Southern California. *Econ. Geol.* **69**, 468–481.

Shen, J. F., Santosh, M., Li, S. R., Zhang, H. F., Yin, N., Dong, G. C., Wang, Y. J., Ma, G. G. and Yu, H. J. (2013) The Beiminghe skarn iron deposit, eastern China: Geochronology, isotope geochemistry and implications for the destruction of the North China Craton. *Lithos* **156–159**, 218–229.

Simmons, S. F., Sawkins, F. J. and Schlutter, D. J. (1987) Mantle-derived helium in two Peruvian hydrothermal ore deposits. *Nature* **329**, 429–432.

Stuart, F. M., Turner, G., Duckworth, R. C. and Fallick, A. E. (1994) Helium isotopes as tracers of trapped hydrothermal fluids in ocean-floor sulfides. *Geology* **22**, 823–826.

Stuart, F. M., Burnard, P. G., Taylor, R. P. and Turner, G. (1995) Resolving mantle and crustal contributions to ancient hydrothermal fluids: He–Ar isotopes in fluid inclusions from Dae Hwa W-Mo mineralisation, South Korea. *Geochim. Cosmochim. Acta* **59**, 4663–4673.

Vallet, J. M., Gosselin, C., Bromblet, P., Rolland, O., Vergés-Belmin, V. and Kloppmann, W. (2006) Origin of salts in stone monument degradation using sulphur and oxygen isotopes: First results of the Bourges cathedral (France). *J. Geochem. Explor.* **88**, 358–362.

Wang, Y. B., Han, J. A. and Zeng, P. S. (2010) U–Pb dating and Hf isotopic characteristics of zircons from granodiorite in Yangla copper deposit, Deqin County, Yunnan, Southwest China. *Acta Petrologica Sinica* **26**, 1833–1844.

Wei, J. Q., Zhan, M. G., Lu, Y. F., Chen, K. X. and He, L. Q. (1997) Geochemistry of granitoids in Yangla ore district, western Yunnan. *Geol. Miner. Resour. South China* **13**, 50–56 (in Chinese with English abstract).

Wei, J. Q., Chen, K. X. and Wei, F. Y. (2000) Tectonism–magmatism–mineralization in Yangla region, western Yunnan. *Geol. Miner. Resour. South China* **1**, 59–62 (in Chinese with English abstract).

Xu, S., Nakai, S. and Wakita, H. (1995) Mantle-derived noble gases in natural gases from Songliao Basin, China. *Geochim. Cosmochim. Acta* **59**, 4675–4683.

Yang, G. Q. (2009) Geological characteristics, genesis and metallogenic prediction of the Yangla copper deposit in Deqin, Yunnan province, China. Ph.D. Thesis, China University of Geoscience, Beijing, 101 pp. (in Chinese with English abstract).

Yang, X. A., Liu, J. J., Cao, Y. and Han, S. Y. (2012) Geochemistry and S, Pb isotope of the Yangla copper deposit, western Yunnan, China: Implication for ore genesis. *Lithos* **144–145**, 231–240.

Yang, X. A., Liu, J. J., Li, D. P., Zhai, D. G., Yang, L. B., Han, S. Y. and Wang, H. (2013) Zircon U–Pb dating and geochemistry of the Linong granitoids and its relationship to Cu mineralization in the Yangla copper deposit, Yunnan, China. *Resour. Geol.* **63**, 224–238.

Zhan, M. G., Lu, Y. F., Chen, S. F., Dong, F. L., Chen, K. X., Wei, J. Q., He, L. Q. and Huo, X. S. (1998) *Yangla Copper Deposit in Deqin, Western China*. China University of Geoscience Publishing House, Wuhan, 179 pp. (in Chinese).

Zheng, Y. F. (1990) Carbon–oxygen isotopic covariation in hydrothermal calcite during degassing of CO_2. *Mineral Deposit* **25**, 246–250.

Zheng, Y. F. and Hoefs, J. (1993) Carbon and oxygen isotopic covariations in hydrothermal calcites. *Mineral Deposit* **28**, 79–89.

Zhu, J., Zeng, P. S., Zeng, L. C. and Yin, J. (2009a) Stratigraphic subdivision of the Yangla copper ore district, northwestern Yunnan. *Acta Geologica Sinica* **83**, 1415–1420 (in Chinese with English abstract).

Zhu, L. M., Zhang, G. W., Li, B., Guo, B., Kang, L. and Lv, S. L. (2009b) Geology, isotope geochemistry and ore genesis of the Maanqiao gold deposit, Shanxi Province. *Acta Petrologica Sinica* **25**, 431–443.